Theory of Coupled Electrochemistry and Piezoelectricity in a Porous Medium

Tianhan Gao[ORCID],[1] Derek Barnes[ORCID],[2] and Wei Lu[ORCID][1,2,*]

[1]*Department of Mechanical Engineering, University of Michigan, Ann Arbor, Michigan 48109, USA*
[2]*Department of Materials Science & Engineering, University of Michigan, Ann Arbor, Michigan 48109, USA*

We find that a porous piezoelectric medium stabilizes electrodeposition and suppresses dendrite. The effect is 6 orders of magnitude larger than mechanical blocking. We develop a theory integrating electrochemistry, piezoelectricity, and mechanics. A piezoelectric overpotential is derived, which reveals a fundamental relation to surface charge density, dielectric property of the medium, electrolyte concentration and diffusivity, and the reaction coefficient. The simulations show that piezoelectric medium suppresses electrodeposition on any protrusion, leading to a flat, dendrite-free surface.

Metallic anodes deliver high theoretical capacity [1–4], but dendrite has limited their application. Take lithium anode as an example. During charging, lithium ions move toward the anode to store energy. Because of unavoidable defects, small protrusions exist on the anode surface. The lithium flux forms a spherical diffusion concentrated toward the tip of protrusion. Therefore, electrodeposition is faster at the tip, leading to needlelike structures called dendrites. They can penetrate the battery separator, causing internal shorting and fire. Theoretical and experimental studies have contributed to understanding dendrite growth [1,5–15]. Several approaches have been proposed to help suppress dendrites, from better ion transport [16–20] to chemically improving the solid-electrolyte interface [21–26] or using electrolyte additives [27–31].

A popular approach independent of cell chemistry is to use a stiff material (e.g., separator, solid-state electrolyte, artificial solid electrolyte interface) to mechanically block dendrite growth. However, the effectiveness remains limited [32–34]. Elastic analysis shows that the required stiffness exceeds the capability of available solid state electrolytes [34]. In fact, the effectiveness is less than the elastic analysis since lithium metal yields. We can estimate a theoretical upper limit by considering an infinitely stiff separator. The principle of mechanical blocking is to generate an overpotential at dendrites tip through mechanical stress to deflect Li ion flux toward other regions to slow down tip growth. This needs to compete against the spherical diffusion concentrated toward the tip. The overpotential by mechanical blocking is $\Omega\sigma/F$ [35,36], where Ω (1.3×10^{-5} m^3 mol^{-1}) is the molar volume of lithium, σ is the magnitude of compressive stress on lithium surface, and F is the Faraday constant. The maximum σ is yield strength, approximately 0.57–1.26 MPa for bulk lithium [37]. These values give an upper limit of mechanical blocking overpotential on the order of 0.1 mV. A representative electrochemical overpotential during lithium deposition is $\sim$10 mV (at current density of 1 mA cm^{-2}) [1]. Comparing these two voltages, we can see that mechanical blocking has little effect in suppressing dendrite since its overpotential is orders of magnitude smaller than the deposition overpotential.

This Letter aims to establish a theory that integrates electrochemistry, piezoelectricity, and mechanics to show a piezoelectric mechanism that ensures dendrite suppression. A piezoelectric separator separates the lithium anode and the counterelectrode. When a dendrite pushes into the separator, a local piezoelectric voltage [35,38] is generated to deflect Li flux away from the tip. To highlight the capability of this mechanism, consider a mild semispherical dendrite of radius r punching into a thin piezoelectric film, stretching an initial flat area of radius r to a dome shape conformal to the semispherical dendrite. The arc length of the dome is πr. The average strain is $(\pi r - 2r)/(2r) =$ 57%. Taking PVDF film as an example, this strain can lead to a piezoelectric voltage of 57 V across the thickness (1 V per 1% strain [38]), which is over 5 orders of magnitude larger than the physical limit of mechanical blocking. A rigorous expression of the ratio of piezoelectric overpotential to mechanical overpotential is derived later, showing over 6 orders of magnitude larger effect. The piezoelectric overpotential is much larger than the 10 mV deposition overpotential, effectively suppressing dendrite.

Figure 1(a) shows *in situ, in operando* observation of lithium deposition on a copper needle, revealing the piezoelectric effect. The counterelectrode is lithium metal, with the electrolyte being LiPF$_6$ in EC:DMC (1:1 vol.%). The semitransparent separator is a porous PVDF film. In the top figure, the film is nonpiezoelectric. In the bottom figure, the film is poled in an electric field to make it piezoelectric before used. All other parameters of the two films are the same as they are cut from the same larger film. Dendrite grows and easily penetrates the nonpiezoelectric film. On the contrary, no dendrite penetration occurs with
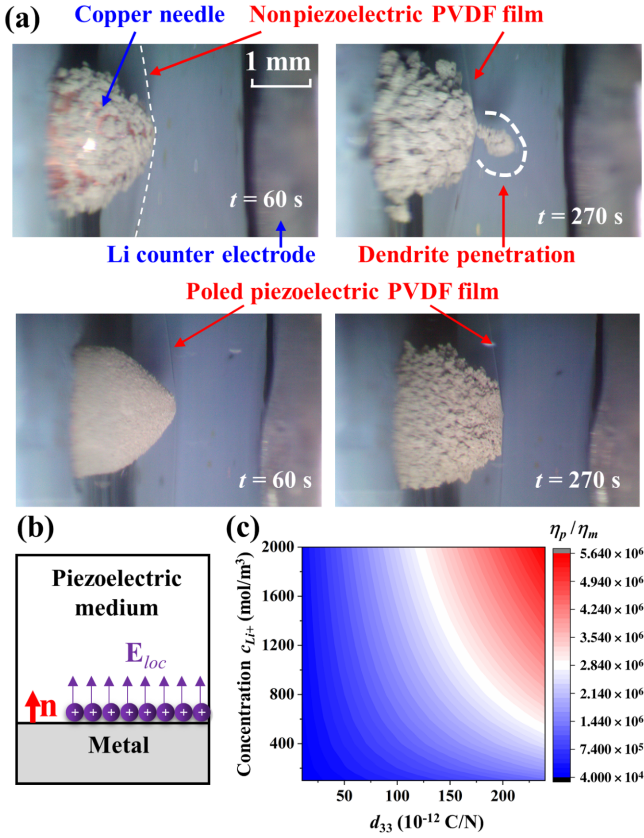
(a) Copper needle Nonpiezoelectric PVDF film

1 mm

$t = 60$ s

$t = 270$ s

Li counter electrode Dendrite penetration

Poled piezoelectric PVDF film

$t = 60$ s

$t = 270$ s

(b)

Piezoelectric medium

$\mathbf{E}_{loc}$

$\mathbf{n}$ +++++++++

Metal

(c)

FIG. 1.   (a) *In situ*, *in operando* observation of lithium deposition on a copper needle under an applied current of 7.5 mA (average current density $\sim$240 mA/cm^2). Dendrite grows and easily penetrates the nonpiezoelectric film (see the white circle at 270 s). On the contrary, no dendrite penetration occurs with the piezoelectric film. (b) Surface charges generated by piezoelectricity affect the local electrochemical reaction. (c) The ratio of piezoelectric overpotential to mechanical overpotential (η_p/η_m) for various piezoelectric constant and ion concentration.

the piezoelectric film, even after a long time. These experimental results show superior dendrite suppression by a piezoelectric medium. This motivates us to establish a theory of dendrite suppression via bulk piezoelectricity in order to open a new avenue to understand the underlying physics and guide the development of new materials.

The traditional electrochemical theory considers ordinary materials. This Letter integrates electrochemistry, piezoelectricity, and mechanics to build a theory for a piezoelectric medium. In a recent work, we assume the piezoelectric film as a zero-thickness mathematical film that generates an electric potential jump proportional to the stretching strain, and show that the piezoelectric potential can significantly affect electrodeposition [38]. This simplification is valid only when the film is extremely thin and also neglects any effect from d_{33} [39]. More importantly, the zero-thickness assumption essentially removes any physical details of coupling between electrochemical kinetics and piezoelectricity since the effect is only a

potential jump. The nanoscale dendrite is typically much smaller than the thickness of a regular separator. Therefore, a bulk theory for the piezoelectric separator is needed since it cannot be simplified as a mathematical film without thickness. In particular, we reveal a fundamental relation of piezoelectric overpotential to surface charge density, dielectric property of the medium, electrolyte concentration and diffusivity, and the reaction coefficient. Such a relation that bridges electrochemistry and the physics of piezoelectric medium will provide an important understanding of how the fields interact with each other.

Consider a generic electrochemical reaction, $M \rightleftarrows M^{n+} + ne^-$, which involves metal M, its ions M^{n+} in the electrolyte and transfer of electron e between the ion and metal. The metal is in contact with a porous piezoelectric medium [Fig. 1(b)]. The fields in the solid piezoelectric phase are described by mechanical-piezoelectric equations with constitutive relations $\boldsymbol{\varepsilon} = \mathbf{C}:\boldsymbol{\sigma} + \mathbf{E} \cdot \mathbf{d}$ and $\mathbf{D} = \mathbf{d} \cdot \boldsymbol{\sigma} + \boldsymbol{\beta} \cdot \mathbf{E}$, where $\boldsymbol{\varepsilon}$, $\mathbf{C}$, $\boldsymbol{\sigma}$, $\mathbf{E}$, $\mathbf{d}$, $\mathbf{D}$, and $\boldsymbol{\beta}$ denote the strain, elastic modulus, stress, electric field, piezoelectric constant, electric displacement, and dielectric constant, respectively. The fields are solved by

$$\nabla \cdot \boldsymbol{\sigma} = \mathbf{0}, \qquad \nabla \cdot \mathbf{D} = \mathbf{0} \qquad (1)$$

Ion transport in the liquid electrolyte phase of the porous media gives

$$\frac{\partial c_i}{\partial t} = -\nabla \cdot \mathbf{N}_i, \qquad (2)$$

$$\mathbf{N}_i = -D_{i,\text{eff}}\nabla c_i - \frac{z_i F D_{i,\text{eff}} c_i}{RT}\nabla \phi_e, \qquad (3)$$

where subscript i denotes species (metal cation, M^{n+}; or anion, $-$), c_i is the concentration of species i in the electrolyte, $\mathbf{N}_i$ is the ion flux, $D_{i,\text{eff}}$ is the effective diffusivity ($D_{i,\text{eff}} = \varepsilon^{1.5} D_i$ with ε and D_i being the electrolyte volume fraction and ion diffusivity), z_i is charge number ($z_{M^{n+}} = n$), R is gas constant, T is temperature, and ϕ_e is electrolyte potential. Charge neutrality requires $z_{M^{n+}} c_{M^{n+}} + z_- c_- = 0$. The current density, $\mathbf{i} = F \sum_i z_i \mathbf{N}_i$, satisfies $\nabla \cdot \mathbf{i} = 0$.

As electrodeposition proceeds, the metal pushes the piezoelectric medium. The elastic field in the metal is described by the mechanics equation. The mechanical interaction between the metal and the piezoelectric medium is solved as a contact problem, which gives the fields in the metal and in the piezoelectric medium.

A key effect of the piezoelectric medium is to generate a surface charge density s at the metal-piezoelectric medium interface [Fig. 1(b)], which affects the local electrochemical reaction. Surface charge density is given by $s = (-\mathbf{n}) \cdot \mathbf{P}$ where $\mathbf{n}$ denotes the normal of contact surface pointing to the piezoelectric medium ($-\mathbf{n}$ is the normal pointing to the metal) and $\mathbf{P} = \mathbf{d} \cdot \boldsymbol{\sigma}$ denotes polarization. Surface charges

add a local electric field $\mathbf{E}_{\text{loc}}$ at the interface, given by Gauss's law

$$\mathbf{E}_{\text{loc}} = \frac{s}{\varepsilon_0 \varepsilon_r} \mathbf{n}, \quad (4)$$

where ε_0 is vacuum permittivity and ε_r is the relative permittivity of electrolyte. To explain the concept, consider that a layer of positive surface charges are generated when a metal protrusion pushes the piezoelectric medium. These charges act as a barrier to resist the deposition of positive metal ions on the protrusion and slow down the tip growth. It should be noted that uniformly placing a layer of charges on the surface of a metal would not help suppress dendrites since it will not selectively slow down the tip growth. This highlights the uniqueness of the piezoelectric mechanism, which selectively slows down deposition onto a protrusion.

The coupling of piezoelectric surface charges and electrochemistry is achieved by adding Eq. (4) into Eq. (3), giving

$$\mathbf{N}_i^{\text{interface}} = -D_{i,\text{eff}} \nabla c_i - \frac{z_i F D_{i,\text{eff}} c_i}{RT} \left(\nabla \phi_e - \frac{s}{\varepsilon_0 \varepsilon_r} \mathbf{n} \right). \quad (5)$$

The boundary conditions at the interface are $\mathbf{N}_{M^{n+}}^{\text{interface}} \cdot \mathbf{n} = i_{M^{n+}}/F$ and $\mathbf{N}_-^{\text{interface}} \cdot \mathbf{n} = 0$, where $i_{M^{n+}}$ is the current density at the interface.

The current density is governed by the Butler-Volmer equation

$$i_{M^{n+}} = FK(c_{M^{n+}})^{1-\alpha} \left[\exp\left(\frac{(1-\alpha)nF\eta_{M^{n+}}}{RT} \right) - \exp\left(-\frac{\alpha n F \eta_{M^{n+}}}{RT} \right) \right], \quad (6)$$

where K is the reaction rate coefficient, α the cathodic symmetrical factor, and $\eta_{M^{n+}}$ the overpotential. Taking the metal potential to be 0, we have $\eta_{M^{n+}} = -\phi_e$. The normal growth velocity of the metal surface due to deposition is $v_n = -\Omega i_{M^{n+}}/F$.

Electrodeposition is solved by coupling the mechanical and piezoelectric field in the piezoelectric medium, the mechanical field in the metal by contact mechanics, ion transport in the medium, the electrochemical reaction at the interface, and the growth of the metal surface (which in turn affects the contact condition and the associated mechanical-piezoelectric fields). In the results shown later, we not only couple all the fields but also include concurrent growth of the solid electrolyte interface (SEI). Details about modeling concurrent deposition growth and SEI growth can be found in our earlier work [1]. With concurrent SEI growth, the boundary conditions become $\mathbf{N}_{M^{n+}}^{\text{interface}} \cdot \mathbf{n} = i_{\text{tot}}/F$, where $i_{\text{tot}} = i_{M^{n+}} + i_{\text{SEI}}$ and i_{SEI} is the SEI reaction current density.

We first understand the piezoelectric effect from a theoretical perspective. Define a piezoelectric overpotential η_p to account for the additional flux from the local electric field of surface charges. Equating the deposition current density, we have

$$K(c_{M^{n+}})^{1-\alpha} \left[\exp\left(\frac{(1-\alpha)nF\eta_{M^{n+}}}{RT} \right) - \exp\left(-\frac{\alpha n F \eta_{M^{n+}}}{RT} \right) \right] + \frac{nFD_{M^{n+},\text{eff}} c_{M^{n+}}}{RT} \frac{s}{\varepsilon_0 \varepsilon_r}$$
$$= K(c_{M^{n+}})^{1-\alpha} \left[\exp\left(\frac{(1-\alpha)nF(\eta_{M^{n+}} + \eta_p)}{RT} \right) - \exp\left(-\frac{\alpha n F(\eta_{M^{n+}} + \eta_p)}{RT} \right) \right]. \quad (7)$$

When the overpotential is small comparing to RT/F, which is typical, we can simplify the equation to $K(c_{M^{n+}})^{1-\alpha} nF\eta_{M^{n+}}/(RT) + nFD_{M^{n+},\text{eff}} c_{M^{n+}} s/(RT\varepsilon_0\varepsilon_r) = K(c_{M^{n+}})^{1-\alpha} nF(\eta_{M^{n+}} + \eta_p)/(RT)$, or

$$\eta_p = \frac{D_{M^{n+},\text{eff}}(c_{M^{n+}})^\alpha s}{K\varepsilon_0\varepsilon_r}. \quad (8)$$

Equation (8) reveals that the piezoelectric overpotential is proportional to the surface charge density, highlighting a fundamental relation between the piezoelectric effect and electrochemical reaction.

Now we compare the piezoelectric effect with mechanical blocking. For a contact pressure of magnitude σ, the piezoelectric effect induces a surface charge $s = d_{33}\sigma$. Note that for suppressing dendrite formation, here we consider the early shallow dendrite morphology so that

the contribution from d_{31} is neglected. When the dendrite is sharper, the contribution from d_{31} becomes significant, further enhancing the piezoelectric effect. With mechanical overpotential $\eta_m = \Omega\sigma/F$, we get $\eta_p/\eta_m = D_{M^{n+},\text{eff}}(c_{M^{n+}})^\alpha d_{33}F/(K\varepsilon_0\varepsilon_r\Omega)$. This ratio is plotted in Fig. 1(c) for lithium metal. The piezoelectric mechanism yields an overpotential 6 orders of magnitude larger than mechanical overpotential in most cases. The ratio increases with d_{33} and cation concentration.

We implemented the developed theory in finite element using COMSOL, and performed fully coupled simulations. The model [Fig. 2(a)] includes a metal in contact with a porous piezoelectric medium, a counterelectrode, and electrolyte in the medium and surrounding the metal. Figure 2(b) shows the evolution of surface morphology during deposition. The effective Young's modulus of the medium is $Y = 500$ MPa. The piezoelectric constant is 50×10^{-12} C/N. The dielectric constant of electrolyte is

$\varepsilon_r = 20$. We can observe that the amount of deposition at the root (quantified by b_B) is much larger than that at the tip (quantified by b_A) where the metal pushes the piezoelectric medium. As electrodeposition continues, the section of metal in contact with the separator becomes flat, indicating that the deposition at the tip is suppressed.

Figure 2(c) compares the morphology at the same time with different piezoelectric constants. Without piezoelectricity ($d_{33} = 0$), the morphology grows slightly sharper. The contact region is more flat with increasing d_{33}, highlighting the dendrite suppression effect. To further understand the interaction, the contact pressure is plotted in Fig. 2(d). The largest pressure is initially at the tip, which is consistent with a Hertzian contact between a cylinder and a flat solid (piezoelectric medium). The larger piezoelectric overpotential reduces deposition at the tip, causing the contact to be flat. Then the location of largest contact pressure gradually shifts to the constant edge. The large pressure concentrated at the contact edge is a signature consistent with a flat block in contact with a flat solid. Similar transition of contact pressure distribution has also been observed during fretting wear between a rod and a flat solid, where the contact surface of the rod wears flat

gradually [40,41]. As the contact edge becomes sharper, the contact pressure there becomes larger. A comparison between the dashed curves ($Y = 500$ MPa, $d_{33} = 25 \times 10^{-12}$ C/N) and solid curves ($Y = 5000$ MPa, $d_{33} = 100 \times 10^{-12}$ C/N) at the same time shows that even with a larger Young's modulus which tends to increase the contact pressure, the larger piezoelectric constant has a stronger effect to suppress the growth and therefore reduces the contact pressure.

We further consider protrusions with different curvatures. The initial shape is semielliptical, with a and b being the semiaxis in the horizontal and vertical direction. We fix b and change a. The ratio a/b reflects sharpness. A larger a/b has a lower curvature at the tip. Figure 3(a) shows that the contact region (FG arc) is much flatter than the noncontact region (HF arc). Figure 3(b) shows that the average curvature of the contact region (FG) becomes significantly smaller than the initial curvature before electrodeposition (DE). Especially for $a/b = 0.7$, the average curvature of FG is only 7.74% of DE. By contrast, the average curvature of the noncontact region has almost no change (HF vs BD). These results highlight that the bulk piezoelectric effect effectively stabilizes
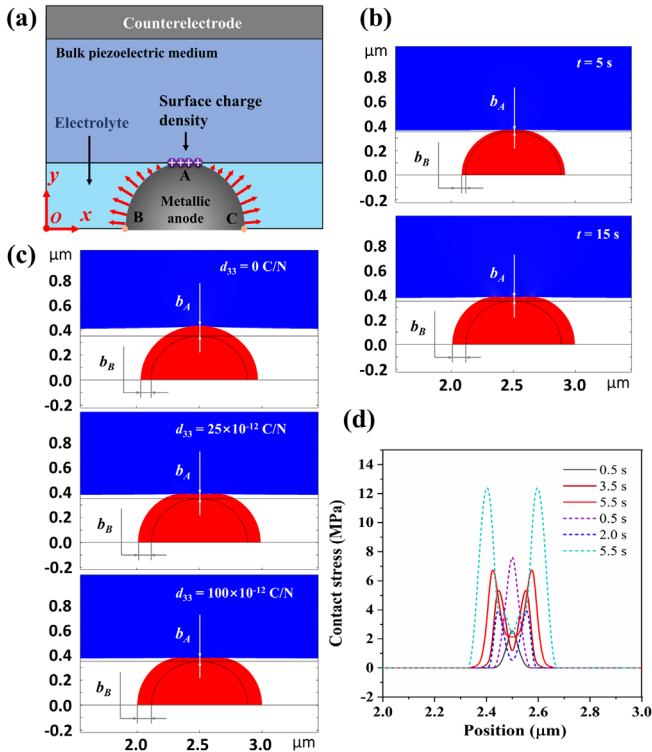

FIG. 2. (a) Model for simulation. (b) Evolution of surface morphology during deposition. (c) Surface morphology at the same time with various piezoelectric constants ($t = 15$ s). (d) Contact pressure on the surface of the piezoelectric medium at different times. (dashed line: $Y = 500$ MPa, $d_{33} = 25 \times 10^{-12}$ C/N; solid line: $Y = 5000$ MPa, $d_{33} = 100 \times 10^{-12}$ C/N).
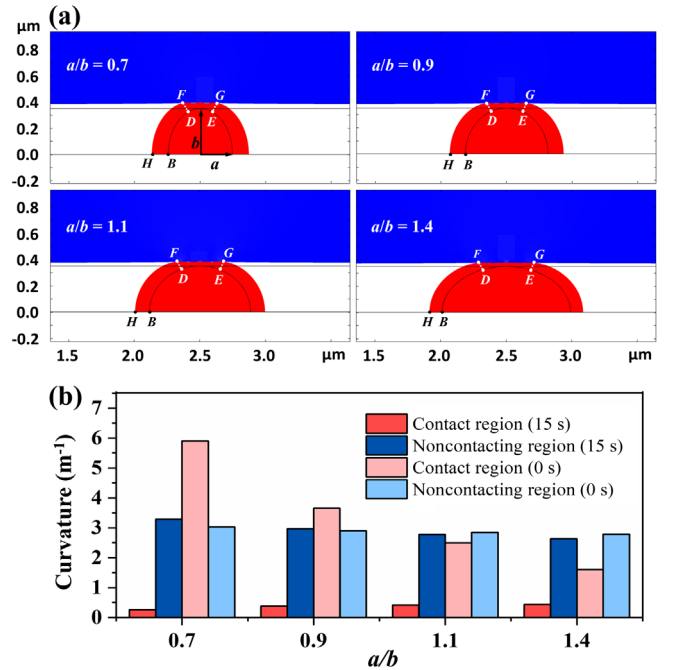

FIG. 3. (a) The morphology of a metal surface starting with various initial curvatures after electrodeposition for $t = 15$ s. ($d_{33} = 50 \times 10^{-12}$ C/N, $\varepsilon_r = 20$, $Y = 500$ MPa). FG denotes the contact region after electrodeposition. DE denotes the initial arc region before electrodeposition that later becomes FG. The other regions, such as BD and HF, are noncontact regions. BD arc is the initial morphology. HF arc is the morphology after electrodeposition. (b) The average curvature of the contact and noncontact regions before and after electrodeposition.
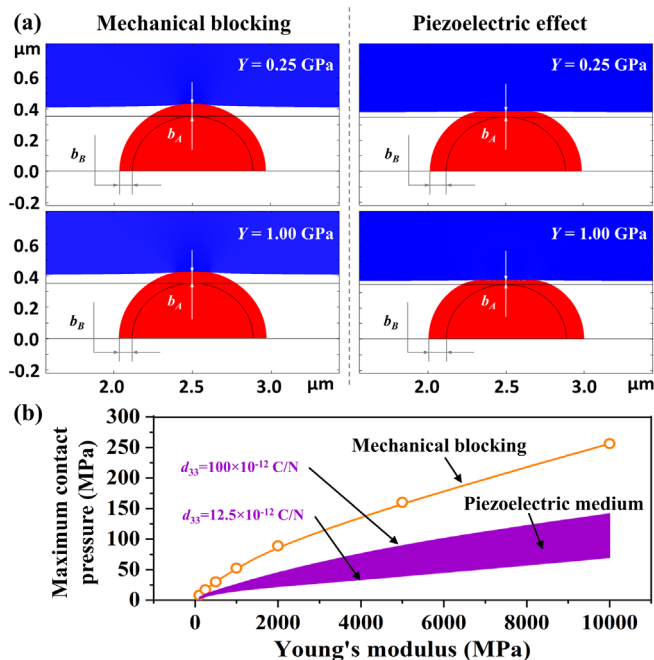
FIG. 4. (a) Comparison of dendrite suppression by the bulk piezoelectric medium and mechanical blocking. Shown is the morphology at $t = 15$ s. For the piezoelectric medium, $d_{33} = 25 \times 10^{-12}$ C/N and $\varepsilon_r = 20$. (b) Maximum contact pressure with various Young's modulus. $t = 15$ s, $\varepsilon_r = 20$.

electrodeposition with various initial surface morphologies, which is vital in preventing nucleation and branching of new dendrites.

We further compare dendrite suppression by the bulk piezoelectric medium and mechanical blocking. Figure 4(a) shows that with Young's modulus up to 1 GPa, mechanical blocking has no visible suppression effect. By contrast, the piezoelectric effect shows a strong effect of electrodeposition stabilization and dendrite suppression (b_A and b_A/b_B are much smaller). Figure 4(b) shows that for various Young's modulus of the medium, the piezoelectric effect always entails a lower contact pressure, which is beneficial for the mechanical integrity of the separator. The yield strength increases at small sizes, which can reach 50–250 MPa for a microscale-nanoscale lithium metal single crystal. The contact pressure from mechanical blocking exceeds 50 MPa when Y reaches 1 GPa and exceeds 250 MPa when Y reaches 10 GPa. Thus lithium metal likely already yields, further reducing the effectiveness of mechanical blocking for dendrite suppression. In contrast, there is a wide range of design space for the piezoelectric mechanism. By using a soft piezoelectric material (e.g., porous PVDF possessing an effective Young's modulus of 200–500 MPa), the contact pressure is much lower than the yield strength of lithium metal.

In conclusion, a bulk piezoelectric medium effectively suppresses dendrite by locally generated charges at the contact. We develop a theory that integrates electrochemistry, piezoelectricity, and mechanics. We show that the overpotential from the bulk piezoelectric medium can be 6 orders of magnitude larger than that of mechanical blocking. A fully coupled numerical approach is implemented using finite element analysis, which couples the mechanical and piezoelectric field in the piezoelectric medium, the mechanical field in the metal by contact mechanics, ion transport in the medium, the electrochemical reaction at the interface, and the growth of the metal surface. Simulations reveal that the piezoelectric mechanism is highly effective in suppressing electrodeposition on the tip of any protrusions or defects, leading to a flat metal surface. This work provides a fundamental understanding of electrochemistry with a porous piezoelectric medium. The model provides guidance on material innovation in this new direction.

———

*weilu@umich.edu

[1] G. Liu and W. Lu, J. Electrochem. Soc. **164**, A1826 (2017).

[2] G. Yoon, S. Moon, G. Ceder, and K. Kang, Chem. Mater. **30**, 6769 (2018).

[3] Z. Hong and V. Viswanathan, ACS Energy Lett. **4**, 1012 (2019).

[4] G. Yasin, M. Arif, T. Mehtab, X. Lu, D. Yu, N. Muhammad, M. T. Nazir, and H. Song, Energy Storage Mater. **25**, 644 (2020).

[5] C. Monroe and J. Newman, J. Electrochem. Soc. **150**, A1377 (2003).

[6] C. Monroe and J. Newman, J. Electrochem. Soc. **151**, A880 (2004).

[7] Y. Liu, X. Xu, M. Sadd, O. O. Kapitanova, V. A. Krivchenko, J. Ban, J. Wang, X. Jiao, Z. Song, J. Song, S. Xiong, and A. Matic, Adv. Sci. **8**, 1 (2021).

[8] A. Aryanfar, S. Medlej, and W. A. Goddard, J. Power Sources **481**, 228914 (2021).

[9] C. Monroe and J. Newman, J. Electrochem. Soc. **152**, A396 (2005).

[10] L. Chen, H. W. Zhang, L. Y. Liang, Z. Liu, Y. Qi, P. Lu, J. Chen, and L. Q. Chen, J. Power Sources **300**, 376 (2015).

[11] H. H. Yan, Y. H. Bie, X. Y. Cui, G. P. Xiong, and L. Chen, Energy Conversion and Management **161**, 193 (2018).

[12] V. Yurkiv, T. Foroozan, A. Ramasubramanian, R. Shahbazian-Yassar, and F. Mashayek, Electrochim. Acta **265**, 609 (2018).

[13] D. Tewari and P. P. Mukherjee, J. Mater. Chem. A **7**, 4668 (2019).

[14] F. Hao, A. Verma, and P. P. Mukherjee, Energy Storage Mater. **20**, 1 (2019).

[15] W. Mu, X. Liu, Z. Wen, and L. Liu, J. Energy Storage **26**, 100921 (2019).

[16] H. Lee, X. Ren, C. Niu, L. Yu, M. H. Engelhard, I. Cho, M. H. Ryou, H. S. Jin, H. T. Kim, J. Liu, W. Xu, and J. G. Zhang, Adv. Funct. Mater. **27,** 1 (2017).

[17] Y. Li, W. Wang, X. Liu, E. Mao, M. Wang, G. Li, L. Fu, Z. Li, A. Y. S. Eng, Z. W. Seh, and Y. Sun, Energy Storage Mater. **23,** 261 (2019).

[18] G. Jiang, K. Li, J. Mao, N. Jiang, J. Luo, G. Ding, Y. Li, F. Sun, B. Dai, and Y. Li, Chem. Eng. J. (Lausanne) **385,** 123398 (2020).

[19] C. Ma, Y. Feng, X. Liu, Y. Yang, L. Zhou, L. Chen, C. Yan, and W. Wei, Energy Storage Mater. **32,** 46 (2020).

[20] K. H. Park, D. W. Kang, J. W. Park, J. H. Choi, S. J. Hong, S. H. Song, S. M. Lee, J. Moon, and B. G. Kim, J. Mater. Chem. A **9,** 1822 (2021).

[21] J. S. Kim, D. W. Kim, H. T. Jung, and J. W. Choi, Chem. Mater. **27,** 2780 (2015).

[22] B. Wu, Q. Liu, D. Mu, H. Xu, L. Wang, L. Shi, L. Gai, and F. Wu, RSC Adv. **6,** 51738 (2016).

[23] G. Wan, F. Guo, H. Li, Y. Cao, X. Ai, J. Qian, Y. Li, and H. Yang, ACS Appl. Mater. Interfaces **10,** 593 (2018).

[24] P. Shi, L. Zhang, H. Xiang, X. Liang, Y. Sun, and W. Xu, ACS Appl. Mater. Interfaces **10,** 22201 (2018).

[25] Y. Yu and X. B. Zhang, Matter Radiat. Extremes **1,** 881 (2019).

[26] Y. Cui, S. Liu, D. Wang, X. Wang, X. Xia, C. Gu, and J. Tu, Adv. Funct. Mater. **31,** 1 (2021).

[27] Z. Hong, Z. Ahmad, and V. Viswanathan, ACS Energy Lett. **5,** 2466 (2020).

[28] A. Bayaguud, X. Luo, Y. Fu, and C. Zhu, ACS Energy Lett. **5,** 3012 (2020).

[29] Y. Zuo, K. Wang, P. Pei, M. Wei, X. Liu, Y. Xiao, and P. Zhang, Mater. Today Energy **20,** 100692 (2021).

[30] X. Guo, Z. Zhang, J. Li, N. Luo, G. L. Chai, T. S. Miller, F. Lai, P. Shearing, D. J. L. Brett, D. Han, Z. Weng, G. He, and I. P. Parkin, ACS Energy Lett. **6,** 395 (2021).

[31] Y. Yang, C. Liu, Z. Lv, H. Yang, Y. Zhang, M. Ye, L. Chen, J. Zhao, and C. C. Li, Adv. Mater. **33,** 1 (2021).

[32] A. Ferrese and J. Newman, J. Electrochem. Soc. **161,** A1350 (2014).

[33] K. J. Harry, K. Higa, V. Srinivasan, and N. P. Balsara, J. Electrochem. Soc. **163,** A2216 (2016).

[34] Z. Ahmad and V. Viswanathan, Phys. Rev. Lett. **119,** 056003 (2017).

[35] G. Liu, D. Wang, J. Zhang, A. Kim, and W. Lu, ACS Mater. Lett. **1,** 498 (2019).

[36] B. Wu and W. Lu, J. Mech. Phys. Solids **125,** 89 (2019).

[37] C. D. Fincher, D. Ojeda, Y. W. Zhang, G. M. Pharr, and M. Pharr, Acta Mater. **186,** 215 (2020).

[38] T. Gao, C. Rainey, and W. Lu, ACS Appl. Mater. Interfaces **12,** 51448 (2020).

[39] J. Yang, *An Introduction to the Theory of Piezoelectricity* (Springer, New York, 2005).

[40] Z. P. Hu, H. Wang, M. D. Thouless, and W. Lu, Int. J. Solids Struct. **139–140,** 302 (2018).

[41] H. Wang, Z. P. Hu, W. Lu, and M. D. Thouless, Nucl. Eng. Des. **318,** 163 (2017).